Applied Catalysis A, General 602 (2020) 117688

Contents lists available at ScienceDirect

Applied Catalysis A, General

journal homepage: www.elsevier.com/locate/apcata

Phosgene formation via carbon monoxide and dichlorine reaction over an activated carbon catalyst: Reaction kinetics and mass balance relationships

Giovanni E. Rossi[a], John M. Winfield[a], Christopher J. Mitchell[b], Nathalie Meyer[c], Don H. Jones[c], Robert H. Carr[c], David Lennon[a,*]

[a] School of Chemistry, Joseph Black Building, University of Glasgow, Glasgow, G12 8QQ, UK
[b] SABIC UK Petrochemicals, The Wilton Centre, Wilton, Redcar TS10 4YA, UK
[c] Huntsman Polyurethanes, Everslaan 45, 3078 Everberg, Belgium

ARTICLE INFO

Keywords:
Phosgene synthesis
Activated carbon
Activation energy
Reaction profile
Mass balance
Rate law

ABSTRACT

The reaction of carbon monoxide and dichlorine over an activated carbon catalyst to produce phosgene is examined using a previously described micro-reactor arrangement. An activation energy of 34.1 kJ mol^{-1} is determined. The reaction profile at 323 K as a function of time-on-stream establishes steady-state operation to be achieved rapidly, with no deactivation evident within a reaction time of 300 min.. Phosgene production seemingly exhibits 100 % selectivity. However, mass balance measurements indicate a small degree of carbon and chlorine retention by the catalyst that is not directly coupled to the formation of gaseous phosgene. The molecular form of the retained moieties is unknown but, nonetheless, their presence reduces the atom economy of the process and, correspondingly, attenuates total phosgene selectivity. The order of reaction with respect CO, Cl_2 and $COCl_2$ is, respectively, 1, 0.5 and 0; leading to the determination of the rate law for phosgene production over this catalyst.

1. Introduction

Phosgene is an important intermediate used in the industrial manufacture of polyurethanes, polycarbonates, pharmaceuticals and agrochemicals [1]. It is typically manufactured industrially *via* the gas phase reaction between carbon monoxide and chlorine over an activated carbon catalyst [2,3].

$$CO_{(g)} + Cl_{2(g)} \rightleftharpoons COCl_{2(g)} \quad (1)$$

The reaction is strongly exothermic ($\Delta H = -107.6$ kJ mol^{-1}) [4].At large-scale industrial chemical complexes, carbon monoxide and chlorine are often supplied *via* purpose-built pipelines such that feeding these reagents as gases into phosgene reactors greatly reduces transportation issues and additional chemical manipulations as might be encountered with alternative manufacturing methods.

Despite wide industrial application, there are surprisingly few laboratory studies of phosgene formation reported in the literature. In 1951 pioneering work from Potter and Baron investigated the reaction kinetics between 298 and 353 K over activated carbon and used a Langmuir–Hinshelwood expression (Eq. 2) to describe the phosgene formation kinetics. The magnitude of the adsorption coefficients was reported as being K_{Cl}, $K_{COCl2} > K_{CO}$ and it was deduced that Cl_2 and $COCl_2$ were physically adsorbed [5].

$$r = k\left[\frac{K_{CO}K_{Cl_2}p_{CO}p_{Cl_2}}{(1 + K_{Cl_2}p_{Cl_2} + K_{COCl_2}p_{COCl_2})^2}\right] \quad (2)$$

In 1956 Weller re-analysed Potter and Barons' data using a model based on power dependencies of the rate with respect to reagent concentrations and proposed the following rate expression (Eq. 3) [6].

$$r = kp_{CO}p_{Cl_2}^{\frac{1}{2}} \quad (3)$$

Over the period 1977–1980 Shapatina and co-workers produced several papers examining the kinetics of the catalytic synthesis of phosgene over activated carbon [7–9], with Eq. 4 being representative of the rate expressions reported,

$$r = kp_{CO}\left(\frac{p_{Cl_2}}{Ap_{CO} + p_{COCl_2}}\right)^{\frac{1}{4}}, \quad (4)$$

where A is a constant.

In 2012 Mitchell and co-workers examined a range of activated carbons for their suitability as phosgene synthesis catalysts [4]. Within that body of work, they used a modified version of Potter and Baron's

* Corresponding author.
E-mail address: David.Lennon@glasgow.ac.uk (D. Lennon).

https://doi.org/10.1016/j.apcata.2020.117688
Received 23 March 2020; Received in revised form 15 May 2020; Accepted 2 June 2020
Available online 06 June 2020

kinetic expression (Eq. 2), as outlined in Eq. 5.

$$r = \frac{k_1\left(P_{CO}P_{Cl2} - \frac{P_{COCl}}{K_{eq}}\right)}{(1 + k_2P_{Cl2})}, \quad (5)$$

where k_1, k_2 and K_{eq} are temperature dependent exponential functions [4]. In 2016 Gupta et al. examined phosgene synthesis over C_{60} fullerene as a model catalyst [10]. Following a combination of experiments backed up by DFT calculations, the authors proposed that retained chlorine reacts rapidly with physisorbed CO *via* a two-step Eley-Rideal type mechanism; an outcome that contrasts with the earlier literature for this process.

The above summary of phosgene synthesis catalysis over the last ~68 years is informative and indicates that there is little consensus for the form of the rate expression associated with the phosgene formation process. Indeed, the most recent work of Gupta and colleagues [10,11] proposes a different class of reaction mechanism compared with the earlier published body of work [3,5–9,12]. Against this background, we have undertaken a kinetic analysis of phosgene synthesis over a representative activated carbon. With reference to the range of catalysts examined by Mitchell and co-workers [4], Donau Supersorbon K40 was selected as being a commercially available activated carbon that was suited to efficient phosgene production, as encountered within certain large-scale isocyanate production chains [13]. A recent article from the authors describes an experimental micro-reactor arrangement plus associated reagent/product-handling protocols for investigating phosgene synthesis catalysts [14]. The facility adopts a similar approach to that recently reported by Tüysüz and co-workers [15], where two independent means of analysis (infrared and UV–vis spectroscopy) are used to precisely characterise aspects of phosgene synthesis. Specifically, this study determines the activation energy for phosgene synthesis over this catalyst and then uses the isolation method to determine the rate law for the reaction. The resulting outcome is compared to the previously reported models (*e.g.* Eq.s 2–5), providing fresh insight as to how the phosgene formation rate is linked to reagent and product concentrations. The experimental protocol adopted [14] additionally lends itself to determination of mass balance relationships. Thus, to the best knowledge of the authors, for the first time, carbon and chlorine mass balances are presented for a defined time-on-stream. An awareness of how mass is partitioned within the reaction network is a necessary perquisite for building a more comprehensive understanding of this commercially relevant reaction system.

2. Experimental

2.1. Phosgene synthesis apparatus

All reactions were performed in the vapour phase on a catalyst test facility described elsewhere [14]. Briefly, in a similar fashion to that described by Tüysüz and co-workers [15], the apparatus utilises in-line FTIR spectroscopy and UV/vis spectrophotometry to speciate and quantify reactants and products for a variety of reaction conditions. All measurements were performed at ambient pressure.

2.2. Catalyst testing

The reactor was typically charged with approximately 0.125 g of Donau Supersorbon K40 of size fraction 250 − 500 μm (Endcotts sieves). The BET surface area and the pore volume of the activated carbon are 1254 $m^2\,g^{-1}$ and 0.579 $cm_3\,g^{-1}$ respectively. Further characterisation details of this material (XRD, Raman spectroscopy, scanning electron microscopy, energy dispersive analysis of X-rays, elemental analysis) are presented elsewhere [14]. For activation, the sample was dried overnight at 383 K in flowing nitrogen (BOC, 99.998 %) at a flow rate of 20 mL min^{-1}; this procedure removed absorbed water.

For reaction testing, the total flow of the exit gas was kept constant at 159 $cm^3\,min^{-1}$; this included a diluent gas flow stream of 100 $cm^3\,min^{-1}$ of dinitrogen entrained at the reactor exit stream that ensured the reagents/products were maintained in the gaseous phase [14]. Hereafter, this additional nitrogen gas flow will be described as the diluent post-reactor gas flow. Adopting a procedure encountered in certain industrial phosgene synthesis facilities [4], the feed-stream of CO and Cl_2 utilised a slight excess of CO. Standard flow conditions were as follows: CO (BOC, CP grade) 5 $cm^3\,min^{-1}$, Cl_2 (Sigma ≥99.5 %) 4 $cm^3\,min^{-1}$, N_2 (carrier gas) 50 $cm^3\,min^{-1}$, and N_2 (diluent post-reactor) 100 $cm^3\,min^{-1}$. The facility is also equipped with a phosgene supply (BOC, 10 % $COCl_2$/He). The initial flow rate (A_0) was determined by passing the gas flow over a by-pass line contained within the oven that contained ground quartz (250 − 500 μm) of comparable volume to the reactor containing catalyst. Once the desired temperature had been attained, the catalyst was exposed to reagents for 20 min before measurements were taken. For variable temperature measurements, 20 min were allowed for the catalyst/reagents to equilibrate thermally before measurements were taken.

2.3. Calibration of reagent/product mixtures at different flow rates

To check the validity of the quantification procedures adopted [14], reagents and products were flowed simultaneously over ~0.125 g ground quartz and monitored spectroscopically at a temperature of 298 K. Three incident flow compositions were examined: (a) 10 $cm^3\,min^{-1}$ 10 % phosgene/He, 6 $cm^3\,min^{-1}$ CO, 4 $cm^3\,min^{-1}$ Cl_2; (b) 20 $cm^3\,min^{-1}$ 10 % phosgene/He, 5 $cm^3\,min^{-1}$ CO, 5 $cm^3\,min^{-1}$ Cl_2; and (c) 30 $cm^3\,min^{-1}$ 10 % phosgene/He, 6 $cm^3\,min^{-1}$ CO, 3 $cm^3\,min^{-1}$ Cl_2. The total flow rate throughout the apparatus was kept constant at 159 $cm^3\,min^{-1}$. Fig. 1 shows a mass balance profile for the detected gases. Although this set of experiments provides no information on the surface chemistry of the reacting system, as no catalyst is present, it does provide a useful consistency check on the calibration procedures adopted.

The left-hand frame of Fig. 1(I) shows how the flow rates of the gases have been varied, whilst the right-hand frame (II) sums the individual components of the detected gas stream in terms of % of molar flow. Reassuringly, frame II shows all three compositions (a, b and c) to return effectively a closed mass balance (± 2 %) in the absence of catalyst, with the error representing one standard deviation of the summed molar flows for the three separate flow measurements. Here, the variance defines the inherent analytical error. The extent of the variance in these measurements will be increased when analysing the catalyst, due to the chemistry thereon adding more complexity and variability with the overall measurement process.

2.4. Activation energy

The reaction between CO and Cl_2 over the activated carbon sample was observed as a function of temperature. The standard reactor gas in-flow [CO 5 $cm^3\,min^{-1}$, Cl_2 4 $cm^3\,min^{-1}$, N_2 (carrier gas) 50 $cm^3\,min^{-1}$] was passed over the by-pass containing ~ 0.125 g ground quartz until stable signals were detected in the infrared and UV–vis spectrometers; these spectral intensities were taken as the A_0 values for each reagent. The gas flow was then switched over the catalyst and left for 20 min before spectral acquisition commenced. The temperature was then increased in 5 K steps from 298 − 323 K and the reaction left for 20 min to stabilise before spectral acquisition commenced. The resulting phosgene flow rate was determined by IR spectroscopy.

2.5. Reaction profile as a function of time-on-stream

The reaction between CO and Cl_2 over Donau Supersorbon K40 was observed as a function of time-on-stream at a temperature of 323 K. The standard reactor gas in-flow [CO 5 $cm^3\,min^{-1}$, Cl_2 4 $cm^3\,min^{-1}$, N_2

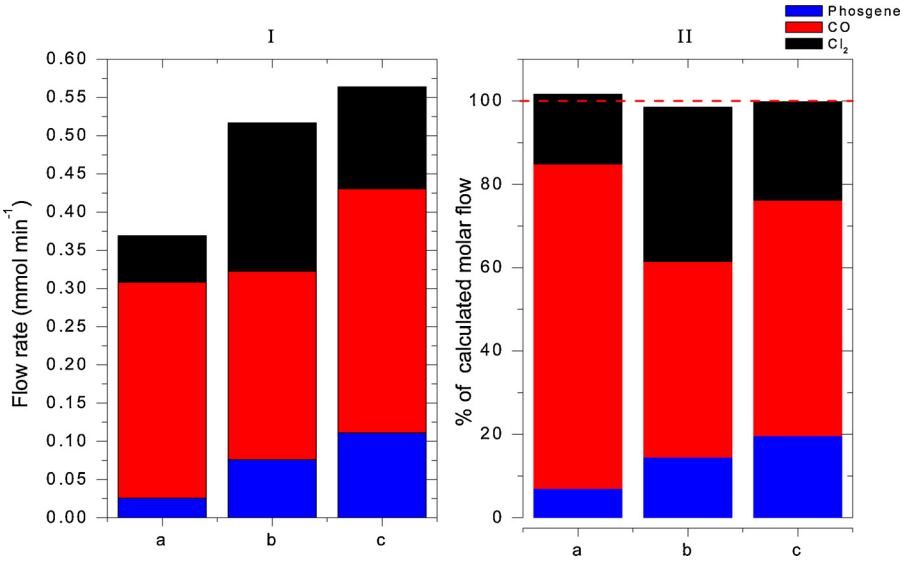

Fig. 1. (I) Mass balance plot of CO, Cl_2 and $COCl_2$ at varying flow rates exiting the by-pass reactor at a temperature of 298 K and (II) the % of the total molar flow rate; *i.e.* reagents are passed over ground and sieved quartz, there is no interaction with the catalyst. Gas flow compositions are as follows: (a) CO 6 $cm^3\,min^{-1}$, Cl_2 1 $cm^3\,min^{-1}$, 10 % $COCl_2$/He 10 $cm^3\,min^{-1}$; (b) CO 5 $cm^3\,min^{-1}$, Cl_2 3 $cm^3\,min^{-1}$, 10 % $COCl_2$/He 20 $cm^3\,min^{-1}$; and (c) CO 6 $cm^3\,min^{-1}$, Cl_2 4 $cm^3\,min^{-1}$, 10 % $COCl_2$/He 30 $cm^3\,min^{-1}$. The red dashed line in (b) represents a complete mass balance (For interpretation of the references to colour in this figure legend, the reader is referred to the web version of this article).

(carrier gas) 50 $cm^3\,min^{-1}$] was passed over the by-pass containing ~ 0.125 g ground quartz until stable signals were detected in the infrared and UV spectrometers; these were taken as the A_0 values for each reagent. The gas flow was switched over to the catalyst and left for 20 min before spectral acquisition commenced. The reaction was then continuously monitored for a period of 300 min. For mass balance measurements (Section 3.3), the first column of the histograms (Figs. 6–8, t < 0 min.) represents gas flow in the absence of the catalyst, *i.e.* through the by-pass reactor (homogeneous chemistry).

2.6. Reaction order

The reaction between CO and Cl_2 over Donau Supersorbon K40 was observed as a function of limiting reagent concentration at a temperature of 323 K. Order dependence for each of the reagents and product was determined by means of the isolation method (v'ant Hoff plots) [16]. This was achieved by fixing one reagent in large excess [15 $cm^3\,min^{-1}$] and varying the flow rate of the limiting reagent [3 – 11 $cm^3\,min^{-1}$] while keeping the volume entering the reactor constant (59 $cm^3\ min^{-1}$) using the front end N_2 carrier gas flow [17]. The effect of phosgene was also examined by fixing CO and $COCl_2$ at 15 cm^3 and varying the 10 % $COCl_2$/He flow rate between 10 – 50 $cm^3\,min^{-1}$, keeping the volume passing through the gas cells constant at 159 $cm^3\,min^{-1}$.

3. Results and discussion

3.1. Activation energy

Fig. 2 presents a sequence of IR spectra obtained as a function of increasing temperature, whilst Fig. 3 presents the equivalent set of UV–vis spectra. Concentrating first on Fig. 2, the A_0 condition for flowing CO and Cl_2 over the by-pass at 298 K yields a spectrum where CO is the only species detected. On switching the reagent feed over the catalyst at 298 K, the IR spectrum changes significantly. CO consumption is evident, whilst peaks at 1824 and 843 cm^{-1} are observed that are respectively assigned to the ν_1(CO) and ν_4(C-Cl) modes of phosgene [14]. Increasing the temperature to 353 K simultaneously diminishes the CO bands, whilst significantly increasing the phosgene features.

Two clear trends are evident in the UV–vis spectrum (Fig. 3). First, increasing temperature leads to a systematic decrease in intensity of the dichlorine $\pi^* \rightarrow \sigma^*$ absorption at 330 nm; second there is a concomitant increase in the phosgene $\pi \rightarrow \pi^*$ absorption at 230 nm. In addition, an isosbestic point is discernible at 272 nm. For a closed system, the

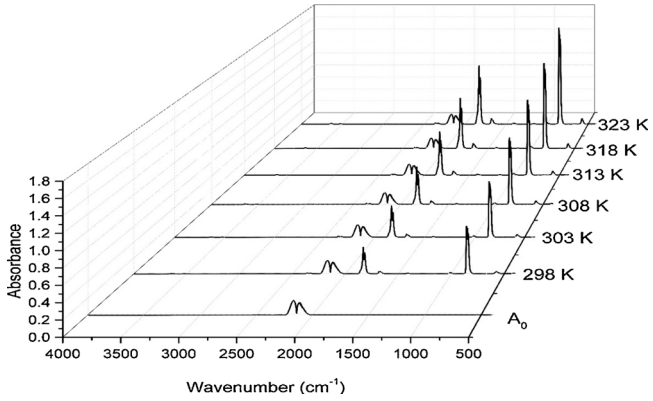

Fig. 2. IR spectra for reaction between CO and Cl_2 over the catalyst as a function of temperature with respective flow rates of 5 $cm^3\,min^{-1}$ and 4 $cm^3\,min^{-1}$ in a total flow of 159 $cm^3\,min^{-1}$ (carrier gas = 50 cm^3 $N_2\,min^{-1}$, diluent post-reactor = 100 cm^3 $N_2\,min^{-1}$) over a temperature range of 298-323 K. The A_0 spectrum corresponds to the reaction mixture passing over quartz in the by-pass reactor at 298 K.

presence of an isosbestic point requires (i) the spectra of the limiting species to intersect and (ii) that changes in the concentration of the various species are linearly related [18]. Fig. 3 shows the $Cl_2 \rightarrow COCl_2$ transformation to adhere to those conditions. No other bands can be distinguished in Fig. 3, signifying that Cl_2 and $COCl_2$ are the only species in the exit stream exhibiting electronic transitions in the 200–600 nm region. Similarly, Fig. 2 shows CO and $COCl_2$ to be the only IR active molecules in the exit stream with absorption in the mid-infrared region of the spectrum. Thus, the phosgene selectivity under these conditions is seemingly 100 %. This matter will be revisited in Section 3.3. Throughout these measurements reagent conversions are maintained at relatively low levels to avoid possible product interference with reaction rate [12]. Specifically, at 298 K CO and Cl_2 conversions are respectively 2 and 4%, increasing to 12 and 25 % at 323 K. That chlorine consumption is in excess of CO will be expanded on in Section 3.2.

Quantification of the spectra presented in Fig. 2 then leads to the Arrhenius plot shown in Fig. 4.

From Fig. 4 the activation energy is calculated to be 34.1 ± 0.2 kJ mol^{-1}, with the error representing the standard error in the overall linear fit. Mitchell and co-workers report activation energies in the range 42 – 50 kJ mol^{-1} for the 8 catalysts they investigated, which is in close correspondence to a value of 56 kJ mol^{-1} reported by Gupta et al.

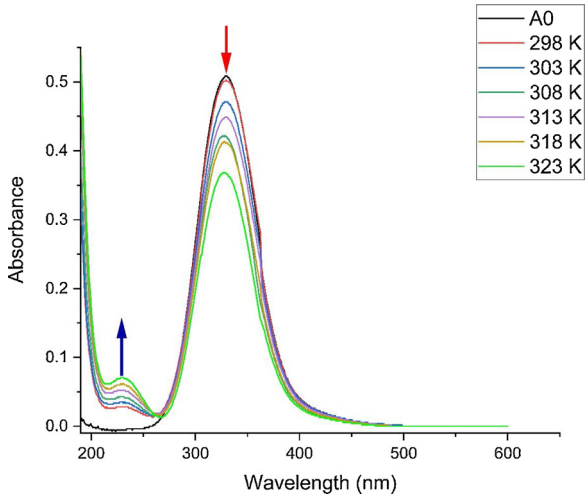

Fig. 3. UV–vis spectra for reaction between CO and Cl_2 over the catalyst as a function of temperature with respective flow rates of 5 $cm^3\,min^{-1}$ and 4 $cm^3\,min^{-1}$ in a total flow of 159 $cm^3\,min^{-1}$ (carrier gas = 50 cm^3 $N_2\,min^{-1}$, diluent post-reactor = 100 cm^3 $N_2\,min^{-1}$) over a temperature range of 298-323 K. The A_0 spectrum corresponds to the reaction mixture passing over quartz in the by-pass reactor at 283 K.

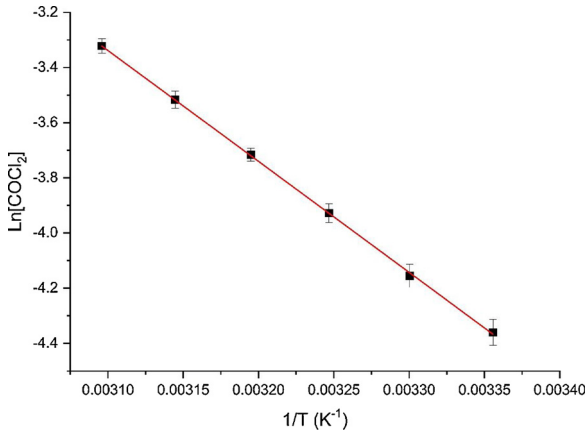

Fig. 4. Arrhenius plot for phosgene formation over Donau Supersorbon K40 over the region 298-323 K. The error bars represent the standard deviation about the mean of three replicate experiments performed at each temperature.

for phosgene formation over a "typical carbon catalyst" [10,11]. However, Shapatina et al. report an activation energy of 36 kJ mol^{-1} over activated carbon, whilst Ajmera et al., report a value of 32 kJ mol^{-1} for Darco G-60 activated carbon examined in a micro-fabricated packed bed reactor [19]; these latter values being comparable to the E_a value reported here for Donau Supersorbon K40. The origins of the disparity in the values of the activation energy are unknown at this time but it is tentatively suggested that it reflects differences in the form of the activated carbons under examination. Nonetheless, a value of 34 kJ mol^{-1} is indicative of the reaction being under kinetic control [20]; an outcome that is consistent with the previously reported absence of inter-phase and intra-phase mass transport contributions in this particular reaction system [14].

3.2. Time-on-Stream

The reaction between CO and Cl_2 over Donau Supersorbon K40 at 323 K was observed as a function of time. The standard reactor incident gas flow [CO 5 $cm^3\,min^{-1}$, Cl_2 4 $cm^3\,min^{-1}$, N_2 (carrier gas) 50 $cm^3\,min^{-1}$] was passed over the by-pass containing ~ 0.125 g ground quartz until stable signals were detected in the infrared and UV

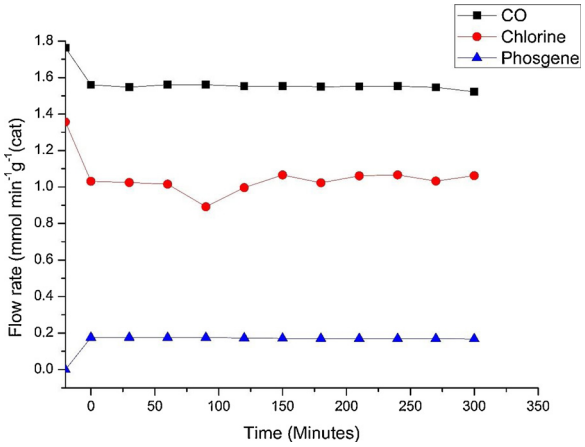

Fig. 5. A plot of CO, Cl_2 and $COCl_2$ flow rates exiting the reactor as CO and Cl_2 are passed over the catalyst at 323 K. Standard gas flow conditions adopted: CO 5 $cm^3\,min^{-1}$, Cl_2 4 $cm^3\,min^{-1}$, N_2 (carrier gas) 50 $cm^3\,min^{-1}$, N_2 (diluent post-reactor) 100 $cm^3\,min^{-1}$.

spectrometers; these were taken as the A_0 values for each reagent. The gas flow was then switched over to the catalyst and left for 20 min before spectral acquisition commenced. The temperature was maintained at 323 K and the reaction left for 20 min before recording spectra in time intervals of 20 min.

Quantification of the spectra leads to the reaction profile shown in Fig. 5. Steady-state operation is achieved quickly (≤ 20 min) and no deactivation is apparent over the 300 min duration of the run. On passing the reagents over the catalyst, mean flow rates of 1.74 (± 0.02) mmol CO $min^{-1}\,g^{-1}_{(cat)}$ and 1.36 (± 0.02) mmol $Cl_2\,min^{-1}\,g^{-1}_{(cat)}$ are observed, with the errors representing one standard deviation for the series of 11 spectroscopic measurements. These flow rates correspond to respective CO and Cl_2 consumptions of 0.21 (± 0.01) and 0.33 (± 0.04) mmol $min^{-1}\,g^{-1}_{(cat)}$. The average rate of phosgene production was 0.172 ± 0.003 mmol $min^{-1}\,g^{-1}_{(cat)}$, with the error (± 1.7 %) similarly defined. This corresponds to a specific activity of 1.37×10^{-5} mmol $m_{(cat)}{}^{-2}$. At steady-state the standard deviation for CO consumption is 4.8 % of the mean flow rate, a value close to the analytical error (Section 2.3). However, the dichlorine value corresponds to 12 % of the mean Cl_2 flow rate, showing a greater variance for this reagent, a factor that may reflect a relatively greater interaction of this reagent with the catalyst and reactor.

The flow rates observed in Fig. 5 correspond to CO and Cl_2 conversions at 323 K of 10.7 and 24.4 % respectively. Thus, in contradiction to Eq. 1 and similar to outcomes reported in Section 3.1, more dichlorine is being consumed than CO. In order to investigate this apparent contradiction further, Section 3.3 examines the mass balance relationships as a function of time-on-stream.

3.3. Mass balance relationships

It is possible to obtain mass balance information from Fig. 5. Firstly, Section 3.3.1. examines the matter of the carbon mass balance, whilst the chlorine mass balance is considered in Section 3.3.2. Finally, Section 3.3.3 considers the overall mass balance profile for reaction at 323 K.

3.3.1. Carbon mass balance

Fig. 6 presents the carbon mass balance plot for CO and $COCl_2$ detected at the exit of the reactor.

Using the scan at 300 min as being representative of the dataset, consumption of CO is 0.24 mmol $min^{-1}\,g^{-1}_{(cat)}$. The $COCl_2$ flow rate is 0.16 mmol $min^{-1}\,g^{-1}_{(cat)}$ that corresponds to a mass imbalance of −0.08 mmol $min^{-1}\,g^{-1}_{(cat)}$, which is −4.6 % of the total CO flow rate.

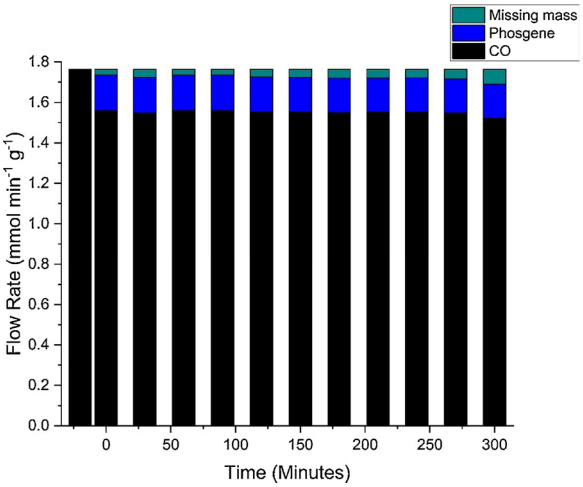

Fig. 6. Carbon mass balance plot determined from CO and $COCl_2$ flow rates exiting the reactor as CO and Cl_2 are passed over the catalyst at 323 K. Standard gas flow conditions adopted: CO 5 $cm^3\,min^{-1}$, Cl_2 4 $cm^3\,min^{-1}$, N_2 (carrier gas) 50 $cm^3\,min^{-1}$, N_2 (diluent post-reactor) 100 $cm^3\,min^{-1}$. The first column (t < 0 min.) represents gas flow in the absence of the catalyst, *i.e.* through the by-pass reactor.

This small mass imbalance is consistent across all 10 scans presented in Fig. 6.

3.3.2. Chlorine mass balance

In order to assess how chlorine is partitioned in the reaction, Fig. 7 presents the chlorine mass balance plot for Cl_2 and $COCl_2$. Here there is some variability between scans; chlorine consumption being higher in the earlier stages of reaction but seemingly asymptoting to a fixed value as the reaction proceeds. Again, taking the 300 min scan as representative, the dichlorine consumption is 0.30 mmol $min^{-1}\,g^{-1}_{(cat)}$, a value that significantly exceeds the observed phosgene flow of 0.17 mmol $min^{-1}\,g^{-1}_{(cat)}$ by 0.13 mmol $min^{-1}\,g^{-1}_{(cat)}$. This missing mass represents −9.6 % of the total dichlorine flow rate. This is in excess of that observed when considering the CO mass balance (Fig. 6) and signifies that the rate of dichlorine consumption is in excess of the rate of

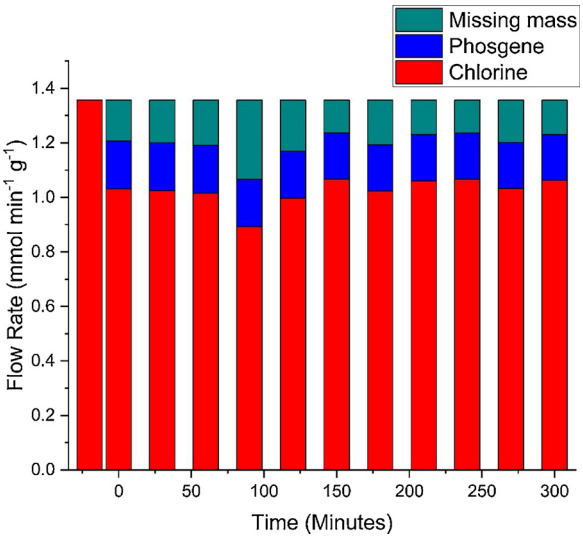

Fig. 7. Chlorine mass balance plot of Cl_2 and $COCl_2$ flow rates exiting the reactor as CO and Cl_2 are passed over the catalyst over at a temperature of 323 K. Standard gas flow conditions: CO 5 $cm^3\,min^{-1}$, Cl_2 4 $cm^3\,min^{-1}$, N_2 (carrier gas) 50 $cm^3\,min^{-1}$, N_2 (diluent post-reactor) 100 $cm^3\,min^{-1}$. The first column (t < 0 min.) represents gas flow in the absence of the catalyst, *i.e.* through the by-pass reactor.

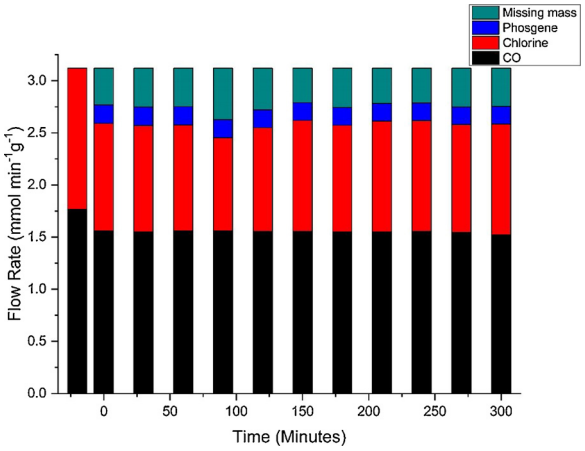

Fig. 8. Overall mass balance plot of CO, Cl_2 and $COCl_2$ flow rates exiting the reactor as CO and Cl_2 are passed over the catalyst over at a temperature of 323 K. Standard gas flow conditions: CO 5 $cm^3\,min^{-1}$, Cl_2 4 $cm^3\,min^{-1}$, N_2 (carrier gas) 50 $cm^3\,min^{-1}$, N_2 (diluent post-reactor) 100 $cm^3\,min^{-1}$. The first column (t < 0 min.) represents gas flow in the absence of the catalyst, *i.e.* through the by-pass reactor.

phosgene production, *i.e.*

$$\frac{-d[Cl_2]}{dt} > \frac{d[COCl_2]}{dt} \tag{6}$$

3.3.3. Total mass balance

The plot for the overall mass balance is presented in Fig. 8.

Adopting 300 min time-on-stream as being representative of steady-state operation (or quasi-steady-state), Fig. 8 shows CO and Cl_2 consumptions to be 0.25 and 0.29 mmol $min^{-1}\,g^{-1}_{(cat)}$ respectively, whilst the $COCl_2$ flow rate is 0.16 mmol $min^{-1}\,g^{-1}_{(cat)}$. On the basis of CO conversion, this corresponds to a deficiency of phosgene formation of 0.09 mmol $min^{-1}\,g^{-1}_{(cat)}$.

The matter of the missing mass now needs to be considered. Fig. 8 only provides information on the gaseous moieties within the reaction system. It is established *via* the closed mass balance presented in Fig. 1 (Section 2.3) that the analytical arrangements can accurately identify and quantify the principal molecules of this reaction system (CO, Cl_2 and $COCl_2$) that are maintained in the vapour phase. The experimental arrangement of a carrier gas in advance of the reactor plus a high flow rate diluent feed entrained with the reactor exit stream ensure that reagents and products of reasonable molecular weight are maintained in the vapour phase [14]. Fig. 8 shows the CO and dichlorine consumption to both exceed the amount of phosgene detected at the rear of the reactor, culminating in an overall mass imbalance at steady-state of 0.37 mmol $min^{-1}\,g^{-1}_{(cat)}$, which corresponds to a mass imbalance of -11.8 % of the total molar flow rate. This analysis leads to the deduction that the mass imbalance evident in Fig. 8 arises from formation of CO and chlorine containing moieties that could either (i) possess significant molecular weight so that they are effectively involatile and thus not detected *via* the gas cells or (ii) are adsorbed on the carbon. The nature of these entities is unknown at this time.

A variety of functional units are present at the surface of activated carbons, such as hydroxyl and carboxyl groups, lactones, phenols, pyrenes, *etc*. [21]. The interaction of carbon and chlorine is a well-established phenomenon [22–27]. Whereas chlorine addition across a non-conjugated double bond will lead to chlorine retention, reactions such as C–H substitution reactions, chloro-dehydrogenation and reactions with hydroxyl groups will yield gaseous HCl or possibly H_2O. The absence of either HCl or H_2O in the infrared spectra of Fig. 2 eliminates a role for those reactions in the chlorine retention process. Alternatively, the additional chlorine consumption could result from the

reaction of chlorine with the carbon surface to produce CCl_4. This reaction is indeed active in large-scale industrial phosgene synthesis facilities [4] that, because of the highly exothermic nature of Eq. 1, can encounter temperatures in excess of 723 K; significantly in excess of temperatures employed in this work, *e.g.* 323 K. However, Fig. 2 shows no evidence for the highly absorbing υ(C-Cl) mode of CCl_4 at 780 cm^{-1}, eliminating the possibility of accessibility of this pathway in our case.

Although it is not possible to state precisely the molecular origins of the mass imbalance observed in Fig. 8, it is deduced that the cause of this small but significant loss of mass is dominated by chlorine retention by the catalyst. Interestingly, Fig. 8 shows that the value for the missing mass component to be approximately constant for the 10 spectroscopic measurements taken over the 300 min. reaction test period. Presumably, for extended reaction times, chlorine adsorption/absorption by the catalyst will saturate and a closed mass balance will result. That outcome was not observed in the present study. Longer-term studies, deemed to be beyond the scope of the present communication, are necessary to investigate this phenomenon further. Nonetheless, it is noted that Shapatina et al.'s post-reaction examination of an activated carbon catalyst applied to phosgene synthesis over the temperature range 343 – 403 K contained 23 wt.% of chlorine [9]. Preliminary EDAX measurements of post-reaction catalyst samples from this work confirm the presence of significant quantities of retained chlorine (> 10 wt%). The adoption of experimental protocols, including a sample passivation procedure, for *ex-situ* chlorine determination in post-reaction samples constitutes work in progress.

Concluding this section, the mass balance profiles indicate that phosgene is not being produced at 100 % selectivity, as implied from Fig. 5 (Section 3.2). Rather, Fig. 8 reveals there to be a degree of carbon and chlorine retention by the catalyst that is not directly coupled to the formation of gaseous phosgene. Although the molecular form of the retained moieties is unknown, nonetheless, their presence reduces the atom economy of the process and, correspondingly, attenuates the phosgene selectivity to < 100 %.

3.4. Order dependence of reagents and product at 323 K

Fig. 9 presents a van't Hoff plot for phosgene formation at 323 K as a function of CO concentration. The data are well described by a linear fit (correlation coefficient R = 0.9989). The individual error bars in Fig. 9 represent the standard deviation from triplicate measurements recorded at five different CO flow rates. The slope of the line corresponds to the order of reaction and was found to be 0.93 ± 0.02, with the error quoted being the standard error in the linear fit for the five datapoints.

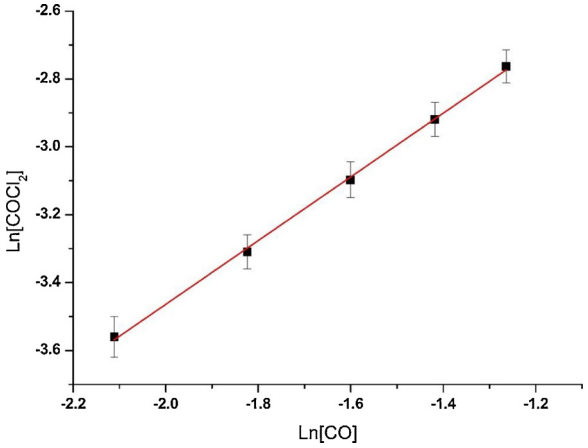

Fig. 9. Ln/ln plot of the concentration dependence of CO for the reaction between CO and Cl_2 over Donau Supersorbon K40 at a reaction temperature of 323 K. Order dependence for CO was determined by fixing chlorine in large excess [15 cm^3 min^{-1}] and varying the flow rate CO [3-11 cm^{-1} min^{-1}] while keeping the volume entering the reactor constant (59 cm^3 min^{-1}) using the front end N_2 flow (carrier gas).

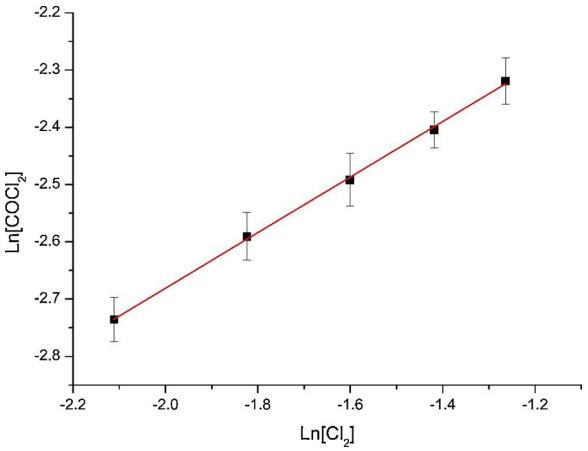

Fig. 10. Ln/ln plot of the concentration dependence of Cl_2 for the reaction between CO and Cl_2 over Donau Supersorbon K40 at a reaction temperature of 323 K. Order dependence for Cl_2 was determined by CO in large excess [15 cm^3 min^{-1}] and varying the flow rate of Chlorine[3-11 cm^{-1} min^{-1}] while keeping the volume entering the reactor constant (59 cm^3 min^{-1}) using the front end N_2 flow (carrier gas).

Fig. 10 presents the corresponding ln/ln plot for phosgene formation rate *versus* dichlorine flow rate. Again the data are well described by a straight line (correlation coefficient R = 0.9989) but now the slope of the line, corresponding to the order of reaction with respect to dichlorine flow rate is 0.48 ± 0.01, with the error being the standard error in the linear fit for the five datapoints.

Fig. 11 presents the v'ant Hoff plot for phosgene production as a function of phosgene flow rate. This is an important measurement as it determines whether the product is rate limiting in this instance. The plot differs significantly from Figs. 9 and 10, which showed phosgene production to be strongly dependent on reagent concentrations. Here, a well correlated linear dependence is seen (correlation coefficient R = 0.999) but exhibiting a slope of -0.04 ± 0.08. Further work is required to determine whether the zero order dependence on phosgene concentration evidenced in Fig. 10 applies to higher conversions.

The order of reagents and product can now be combined to provide the experimentally determined rate law for this reaction, Eq. 7.

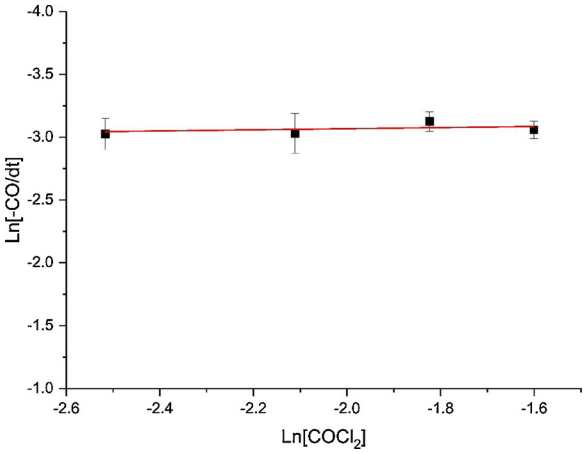

Fig. 11. Plot of the log of the concentration dependence of $COCl_2$ for the reaction between CO and Cl_2 over Donau Supersorbon K40 at a reaction temperature of 323 K. Order dependence for $COCl_2$ was determined by both CO and Cl_2 in large excess [15 cm^3 min^{-1}] and varying the flow rate of 10 % $COCl_2$/He between 10-50 cm_3 min^{-1}, while keeping the volume entering gas cells constant (159 cm^3 min^{-1}) by varying the front end N_2 flow (carrier gas).

$$v = k[CO]^{0.93\pm0.02}[Cl_2]^{0.48\pm0.01}[COCl_2]^{-0.04\pm0.08}, \quad (7)$$

where k represents a rate coefficient. Within experimental error, Eq. 7 can be simplified to Eq. 8,

$$v = k[CO]^{1}[Cl_2]^{0.5}[COCl_2]^{0} \quad (8)$$

Eq. 8 shows distinct values for each of the constituent molecules. CO is shown to be first order, in contrast to dichlorine that exhibits a half-order dependence. With reference to Eq. 1, it is tempting to suggest that the CO involvement in the phosgene formation process involves molecular adsorption but that dichlorine involves dissociative adsorption over the activated carbon catalyst. Phosgene is different again, exhibiting a zero order dependence on reaction rate, signifying that there to be no product retardation with this reaction. This combination of outcomes is favourable for efficient catalysis.

It is informative to compare Eq. 8 with the rate expressions reported for other studies of phosgene synthesis catalysis as outlined in the Introduction. As the majority of the previously reported rate expressions utilise Langmuir-Hinshelwood expressions, it is easier to correlate Eq. 8 with the simple power law dependence adopted by Weller (Eq. 3) that was able to more accurately account for the experimental outcomes reported by Potter and Barron [6]. Unfortunately, Weller's analysis did not include an expression for the product but, that aside, Eq. 3 similarly reports a first order dependence on CO concentration and a half-order dependence on dichlorine concentration. Eq. 8 shows zero order dependence on phosgene. As Eq. 3 was able to more accurately account for Potter and Barron's experimental data than their own expression (Eq. 2), this implies that phosgene would have to be zero order in Eq. 3 to achieve such favourable correlation with the Potter and Barron dataset, *i.e.* Eqs. 3 and 8 are equivalent. Thus, in this way, this work has, to a degree, brought clarity to the matter of probable rate expressions for this reaction. Certainly, for phosgene synthesis over the activated carbon catalyst under investigation here, Eq. 8 leads to a relatively straight-forward kinetic description that accounts for the observed rates of phosgene synthesis with minimal product retardation, as implicated in some of the Langmuir-Hinshelwood expressions. Furthermore, as pointed out by Weller [6], the relatively simpler mathematical expression of Eq. 8 avoids the problem of accurately determining the adsorption coefficients that is required by the Langmuir-Hinshelwood methodology.

4. Conclusions

A previously described experimental facility [14] has been used to examine the kinetics of phosgene synthesis from the reaction of carbon monoxide and dichlorine over a commercial grade activated carbon catalyst (Donau Supersorbon K40) at ambient pressure and relatively low temperatures (298 − 323 K). The following conclusions can be drawn.

- Phosgene synthesis exhibits an activation energy of 34.1 ± 0.2 kJ mol^{-1}.
- The reaction profile establishes steady-state operation to be achieved rapidly (≤ 20 min. time-on-stream) with no deactivation evident but, in contrast to the stoichiometric equation for phosgene synthesis, dichlorine consumption exceeds that observed for CO.
- The carbon mass balance profile establishes CO consumption to fractionally exceed the rate for phosgene formation, corresponding to a carbon mass imbalance of -4.6 % at quasi-steady state operation.
- The chlorine mass balance profile establishes dichlorine consumption to exceed the rate for phosgene formation, corresponding to a chlorine mass imbalance of −9.6 % at quasi-steady state operation
- The overall mass balance plot reveals a mass imbalance of −12 % of the total molar flow rate. This imbalance is attributed to the formation of CO and chlorine containing moieties that could either (i) possess significant molecular weight so that they are effectively involatile and thus not detected *via* the gas cells, or (ii) are adsorbed on the carbon. The nature of these entities is unknown at this time.
- The retention of feedstock by the catalyst reduces the atom economy of the process and, correspondingly, attenuates the phosgene selectivity to < 100 %.
- The rate law for the reaction has been determined and is consistent with that previously reported by Weller [6].

CRediT authorship contribution statement

Giovanni E. Rossi: Data curation, Formal analysis, Investigation, Methodology, Software, Writing - original draft, Writing - review & editing. **John M. Winfield:** Formal analysis, Investigation, Methodology, Supervision, Validation, Writing - review & editing. **Christopher J. Mitchell:** Conceptualization, Funding acquisition, Methodology, Project administration, Resources, Writing - review & editing. **Nathalie Meyer:** Formal analysis, Methodology, Project administration. **Don H. Jones:** Formal analysis, Methodology, Validation, Writing - review & editing. **Robert H. Carr:** Conceptualization, Funding acquisition, Project administration, Resources, Writing - review & editing. **David Lennon :** Formal analysis, Investigation, Methodology, Project administration, Supervision, Validation, Writing - original draft, Writing - review & editing.

Declaration of Competing Interest

The authors declare that they have no known competing financial interests or personal relationships that could have appeared to influence the work reported in this paper.

Acknowledgements

The College of Science and Engineering (GU), the School of Chemistry (GU) and Huntsman Polyurethanes are thanked for project support and the provision of a pH.D studentship (GER). The EPSRC are additionally thanked for equipment support *via* a Knowledge Exchange award (EP/H500138/1).

Appendix A. Supplementary data

Supplementary material related to this article can be found, in the online version, at doi:https://doi.org/10.1016/j.apcata.2020.117688.

References

[1] R. Lin, A.P. Amrute, J. Pérez-Ramírez, Chem. Rev. 117 (2017) 4182–4247, https://doi.org/10.1021/acs.chemrev.6b00551.
[2] J. Davy, Philos. Trans. R. Soc. London. 102 (1812) 144–151, https://doi.org/10.1098/rstl.1812.0008.
[3] T.A. Ryan, E.A. Seddon, K.R. Seddon, C. Ryan, Phosgene: And Related Carbonyl Halides, Elsevier Science, 1996.
[4] C.J. Mitchell, W. van der Borden, K. van der Velde, M. Smit, R. Scheringa, K. Ahrika, D.H. Jones, Catal. Sci. Technol. 2 (2012) 2109, https://doi.org/10.1039/c2cy20224g.
[5] C. Potter, S. Baron, Chem. Eng. Prog. 47 (1951) 473–481.
[6] S. Weller, Am. Inst. Chem. Eng. J. 2 (1956) 59.
[7] E.N. Shapatina, V.L. Kuchaev, M.I. Temkin, React. Kinet. Catal. Lett. 20 (1978) 972–976.
[8] E.N. Shapatina, V.L. Kuchaev, M.I. Temkin, React. Kinet. Catal. Lett. 18 (1977) 968–972.
[9] E.N. Shapatina, V.L. Kuchaev, B.E. Pen'kovoi, M.I. Temkin, React. Kinet. Catal. Lett. 17 (1976) 559–566.
[10] N.K. Gupta, A. Pashigreva, E.A. Pidko, E.J.M. Hensen, L. Mleczko, S. Roggan, E.E. Ember, J.A. Lercher, Angew. Chemie - Int. Ed. (2016) 1728–1732, https://doi.org/10.1002/anie.201508922.
[11] N.K. Gupta, B. Peng, G.L. Haller, E.E. Ember, J.A. Lercher, ACS Catal. 6 (2016) 5843–5855, https://doi.org/10.1021/acscatal.6b01424.
[12] C.N. Satterfield, Heterogeneous Catalysis in Industrial Practice, reprint ed, Krieger Publishing Company, 1996.
[13] E.K. Gibson, J.M. Winfield, D. Adam, A.A. Miller, R.H. Carr, A. Eaglesham,

D. Lennon, Ind. Eng. Chem. Res. 53 (2014) 4156–4164.
[14] G.E. Rossi, J.M. Winfield, C.J. Mitchell, W. van der Borden, K. van der Velde, R.H. Carr, D. Lennon, Appl. Catal. A Gen. 594 (2020) 117467.
[15] A. Bähr, G.-H. Moon, J. Diedenhoven, J. Kiecherer, E. Barth, H. Tüysäuz, Chem. Ing. Tech. 90 (2018) 1513.
[16] P. Atkins, J. De Paula, Atkins' Physical Chemistry, 9th edition, Oxford University Press, 2010.
[17] P. Atkins, J. De Paula, The Elements of Physical Chemistry, 5th edition, Oxford University Press, 2009.
[18] C.G.A. Morisse, A.R. McInroy, C. Anderson, C.J. Mitchell, S.F. Parker, D. Lennon, Catal. Today 283 (2017) 110–118.
[19] S.K. Ajmera, M.W. Losey, K.F. Jensen, M.A. Schmidt, AIChE J. 47 (2001) 1639–1647.
[20] C.H. Bartholomew, R.J. Farrauto, Fundamentals of Industrial Catalytic Processes, second ed, Wiley, 2006.
[21] D. Lennon, D.T. Lundie, S.D. Jackson, G.J. Kelly, S.F. Parker, Langmuir 18 (2002) 4667–4673.
[22] J. González, M.C. Del Ruiz, A. Bohé, D. Pasquevich, Carbon 37 (1999) 1979–1988.
[23] C. Hall, R.J. Holmes, Carbon 30 (1992) 173–176.
[24] D.M. Pasquevich, Thermochim. Acta 167 (1990) 91–98.
[25] H. Tobias, A. Soffer, Carbon 23 (1985) 281–289.
[26] H. Tobias, A. Soffer, Carbon 23 (1985) 291–299.
[27] A.F. Pérez-calenas, F.J. Maldonado-Hódar, C. Moreno-Castilla, Carbon 41 (2003) 473–478.